ADVANCED ENERGY MATERIALS
www.advenergymat.de

Understanding Power-Law Photoluminescence Decays and Bimolecular Recombination in Lead-Halide Perovskites

Ye Yuan, Genghua Yan, Chris Dreessen, and Thomas Kirchartz**

Transient photoluminescence is a frequently used method in the field of halide perovskite photovoltaics to quantify recombination by determining the characteristic decay time of an exponential decay. This decay time is often considered to be a single value for a certain perovskite film. However, there are many mechanisms that lead to non-exponential decays. Here, it is shown that photoluminescence decays in many lead-halide perovskites are non-exponential and follow a power-law relation between PL intensity and time that is caused by shallow defects. Decay times therefore vary continuously as a function of time and injection level. In situations where recombination is bimolecular and decays follow a power law, the differential decay time equals the time delay after the laser pulse for long time delays and therefore completely lacks quantitative information about the recombination rate. Quantifying recombination using transient PL measurements, therefore, requires analyzing the lifetime as a function of injection level rather than time. As an alternative to the continuously varying decay time, a bimolecular recombination coefficient can also be determined, which correlates with the photoluminescence quantum efficiency. Finally, the influence of the repetition rate and the background subtraction method on the analysis of power-law type PL decays is discussed.

1. Introduction

The combination of ease of fabrication[1] with outstanding electronic properties[2] has made lead-halide perovskites an extremely popular research topic for applications in photovoltaics and optoelectronics.[3] The most remarkable feature of this material class is the relatively low share of non-radiative recombination, which manifests experimentally in high photoluminescence quantum yields[4] and high open-circuit voltages relative to the bandgap of the absorber material.[5] The characterization of recombination in halide perovskite films, layer stacks, and devices is primarily achieved using transient and steady-state photoluminescence methods that are used in a large share of experimental publications on halide perovskites.[6] In particular, transient photoluminescence (tr-PL) is a frequently used and likely also frequently misinterpreted method. Despite the abundant use of the method in the literature, there are no standards on how to analyze the experimental data so far. This is a situation that is strikingly different from the state-of-the-art, for example, in silicon photovoltaics, where lifetime spectroscopy has been largely standardized after the development of the quasi-steady-state photoconductance technique.[7]

The basic idea of tr-PL is to excite the sample (typically a perovskite film on glass) with a laser pulse and to record the photoluminescence as a function of time. The decay is often analyzed using exponential or multi-exponential fitting[8] and charge-carrier lifetimes are extracted, which are used as figures of merit for non-radiative recombination.[9] The measurement equipment is nearly always based on the time-correlated single-photon counting (TCSPC) technique, which makes use of a high number of repetitions of the same measurement to build up statistical data about the time delay between the laser pulse and the detection of a photon.[10] Thus, high repetition rates are useful to achieve good signal-to-noise ratios and short measurement times. The inverse repetition rate, that is, the time between two pulses, is an important consideration as it cuts off the decay and may lead to a pile-up of charge carriers, thereby affecting the physics and the analysis of the measurement.[11] As lead-halide perovskites have extremely low doping densities,[12] recombination is typically nonlinear with charge-carrier density. Only in the limiting case where the decay is dominated by recombination via a midgap defect would tr-PL decay exponentially. In the presence of radiative recombination,[13] shallow defects,[14] and diffusion effects,[15] recombination decays non-exponentially, and the decay may often resemble a power law between photoluminescence intensity and time.[14,16] In this situation, the determined lifetime critically

Y. Yuan, G. Yan, C. Dreessen, T. Kirchartz
IMD3-Photovoltaik
Forschungszentrum Jülich
52425 Jülich, Germany
E-mail: ge.yan@fz-juelich.de; t.kirchartz@fz-juelich.de
T. Kirchartz
Faculty of Engineering and CENIDE
University of Duisburg-Essen
Carl-Benz-Str. 199, 47057 Duisburg, Germany

The ORCID identification number(s) for the author(s) of this article can be found under https://doi.org/10.1002/aenm.202403279

DOI: 10.1002/aenm.202403279

depends on the excitation density[14] and repetition rate, and the consideration of these two parameters is crucial for a meaningful analysis and interpretation of the data as we will outline in detail in this article.

The starting point of this work is our recent observation that the transient PL curves of typical lead-halide perovskites are dominated by higher-order recombination. From the solution of the differential equation for a recombination rate that is quadratic in carrier density, one immediately arrives at the conclusion that they should exhibit a power-law decay for high fluences and an exponential decay only for low fluences.[14] Based on our empirical evidence obtained so far (shown in this work and from references[14,17]), this observation seems to be general for a variety of different lead-halide perovskite compositions measured at sufficiently high fluences. The power law only becomes visible if the measurement is performed over a sufficient dynamic range and the data is plotted on a double-logarithmic scale. As literature data is rarely measured with a high dynamic range and the used fluences are often rather low, this observation of power-law decays is difficult to make by studying the existing literature.

In this article, we discuss the consequences of power-law decays both experimentally and analytically. A mathematical consequence of this effect is that the extracted decay time changes depending on the charge-carrier concentration and the delay time. The consequence of this finding is that a determination of single lifetimes for a lead-halide perovskite film would not contain any meaning except the carrier density at which the lifetime is taken was stated. As this is not typically done, lifetime values determined from tr-PL decays would rarely be suitable to provide a quantitative measure of recombination. Furthermore, unlike PL quantum efficiencies that can be used to compare samples across different publications, a meta-analysis of published charge-carrier lifetimes only poorly correlates with actual electronic quality as the measurement conditions would likely vary from paper to paper.[6a] We show that the use of effective bimolecular recombination coefficients can be a viable solution to simplify data analysis and inter-sample comparisons in those situations, where the decay is following a power law rather than a single or multi-exponential decay.

2. Theory of Charge-Carrier Recombination and tr-PL Decays

In the following, we will briefly discuss why the PL intensity of a lead halide perovskite film as a function of time after a laser pulse could decay exponentially, as a power law, or a combination of both. We furthermore explain how such decays can be quantitatively analyzed. Given that lead-halide perovskites behave like intrinsic semiconductors,[12] the luminescence is generally measured under high-level injection. At time 0 after the excitation pulse, the electron concentration n and hole concentration p are equal, $n = p$. Afterward, unequal trapping of charge carriers may change that and lead to photodoping. Neglecting Auger recombination for simplicity, we consider radiative recombination and Shockley-Read-Hall (SRH) recombination[18] as recombination mechanisms. For SRH recombination, we look here at the two simplified cases of deep defects and shallow defects.

In general, defects can be charged and can thereby change the ratio of electron and hole densities even in a semiconductor that is undoped in the dark. While this concept of photodoping will be important to understand power-law decays, let us initially study the simplified case, where the density of deep defects is sufficiently low that its charge density does not affect the Poisson equation and thereby the charge neutrality condition of our perovskite film. In this simple case, the condition $n = p$ will always be fulfilled, and we do not need to distinguish between electrons and holes. The time derivative of the carrier concentration for a combination of radiative recombination and SRH recombination via a deep defect is then given by[6a]

$$-\frac{dn}{dt} = \left[k_{\mathrm{rad}} n^2 + \frac{n}{\tau_{\mathrm{SRH}}}\right] \tag{1}$$

where n, k_{rad} and τ_{SRH} are the electron concentration, radiative recombination coefficient and SRH lifetime, respectively. The SRH lifetime is the sum of the electron SRH lifetime and the hole SRH lifetime, $\tau_{\mathrm{SRH}} = \tau_{\mathrm{SRH,n}} + \tau_{\mathrm{SRH,p}}$. The solution of Equation (1) for $n(t)$ can be written as[6a]

$$n(t) = \frac{n(0)\exp\left(-t/\tau_{\mathrm{SRH}}\right)}{1 + n(0)\,k_{\mathrm{rad}}\tau_{\mathrm{SRH}}\left[1 - \exp\left(-t/\tau_{\mathrm{SRH}}\right)\right]} \tag{2}$$

where $n(0)$ is the initial carrier concentration after the infinitely short laser pulse has been absorbed. The PL intensity should then scale with the square of the time-dependent carrier density given by Equation (2). For low values of the SRH lifetime τ_{SRH} (corresponding to high non-radiative recombination), the carrier density decays exponentially as only the numerator matters and the denominator is approximately one, leading to

$$n(t) = n(0)\exp\left(-t/\tau_{\mathrm{SRH}}\right) \tag{3}$$

However, for higher values of τ_{SRH} (corresponding to low non-radiative recombination via deep defects), the second term in the denominator will dominate. If the SRH lifetimes are long enough to Taylor-expand the exponentials, we would obtain

$$n(t) = \frac{n(0)}{1 + n(0)\,k_{\mathrm{rad}}t} \approx \frac{1}{k_{\mathrm{rad}}t} \tag{4}$$

whereby the term after the ≈ sign is for the case, where the time $t \gg 1/[n(0)k_{\mathrm{rad}}]$. Thus, Equation (2) describes a continuous transition from an exponential decay to power-law decay depending on the values of k_{rad} and τ_{SRH}. Despite this fact, the overwhelming majority of experimental data on halide perovskite films is analyzed assuming exponential decays without validating the assumption. Often, an equation of the form $y = y_0 + A_1 e^{-x/\tau_1} + A_2 e^{-x/\tau_2}$ is fitted to the data. This does not reflect the mathematics of Equation (2) but it is understandable from a practical point of view as single- and multiexponential fitting is often quite stable and already pre-implemented in many data analysis tools. Furthermore, the constant offset y_0 takes care of the apparent noise floor and enables a good fit even if no efforts were invested in measuring and subtracting the noise. A downside of the approach is that there is no obvious physical meaning of the parameters y_0, A_1, A_2, τ_1 and τ_2. They could not, for instance, be directly related to parameters such as k_{rad} and τ_{SRH}.

An alternative to directly fitting the PL decay is to first determine a quantity that is easier to interpret and that can be directly derived from experimental data, that is, without fitting or assuming any physical model. Previously, we have therefore introduced the differential decay time τ_{diff} that is defined as[17]

$$\tau_{\mathrm{diff}} \equiv -\frac{2dt}{d\ln\phi\,(t)} \tag{5}$$

Note that the differential decay time is intended to be a direct result of the experimental observables PL intensity ϕ and delay time t and that physical models (e.g., rate equation models) can be fitted to the differential decay time to further corroborate physical explanations. Furthermore, the logic of Equation (5) is extremely similar to the approaches that have been used, for example, in the silicon photovoltaic community for decades.[19] Here, we intentionally only use the word "lifetime" for model-based parameters such as τ_{SRH} to distinguish them from the decay times derived directly from the experiment. The definition provided in Equation (5) originates from the idea that in an intrinsic semiconductor without photodoping ($n = p$), the PL intensity is proportional to n^2. Hence, the differential decay time follows from Equation (1) via

$$\tau_{\mathrm{diff}} = -\frac{n\,(t)}{\frac{dn(t)}{dt}} = \frac{1}{k_{\mathrm{rad}}n\,(t) + \frac{1}{\tau_{\mathrm{SRH}}}} \tag{6}$$

And thereby directly assigns physical meaning to the dependence of the differential decay time to the charge carrier density. The prediction is that the decay time has two components, one that inversely depends on carrier density and that results from the power-law part of the decay and one that is independent of carrier density and represents the exponentially decaying part of the PL with τ_{SRH}. However, the differential decay time can be applied to any decay as it has the advantage that it does not impose any physical model a priori but rather gives indications of which model may be the correct one to use based on the dependence of the decay time on carrier density. Note that one can define the electron and hole lifetimes $\tau_{\mathrm{n}} \equiv -n(t)/(dn(t)/dt)$ and $\tau_{\mathrm{p}} \equiv -p(t)/(dp(t)/dt)$ which are equal to τ_{diff} for the assumed case of $n = p$.

As we will see in the following, the simplified analysis done above has one key shortcoming which lies in the assumption that the defects are deep and do not contribute any charge density to the charge neutrality condition. In the case where shallow traps are present in the material, Equations (1) to (3) will not describe the decay anymore and there is no universal analytical equation anymore to describe the complete time dependence of the electron density. The difference between shallow and deep defects is that detrapping to the nearest band is more likely to happen. At early times after a laser pulse hits the semiconductor, trapping and detrapping occur at different rates, resulting in complicated charge carrier dynamics. After a certain time that depends on the depth of the trap, the rates of trapping and detrapping to the nearest band will have become similar and the decay will proceed in a fashion that can approximately be described using analytical equations. These equations depend on assumptions such as the density and charge state of the defects. Contrary to the case of deep traps, we discuss here the case of a high density of traps, so that trapped charges affect the charge neutrality condition and photodoping may occur ($n \neq p$). In the case of a high density of shallow acceptor-like traps close to the conduction band, the differential equation determining the electron density follows as (see Note S2, Supporting Information for derivations),

$$-\frac{dn}{dt} = \frac{1 + k_{\mathrm{rad}}\tau_{\mathrm{SRH,p}}n_1}{\tau_{\mathrm{SRH,p}}n_1}\,n^2 = k_n n^2 \tag{7}$$

where $n_1 = N_{\mathrm{C}}\exp[(E_{\mathrm{T}} - E_{\mathrm{C}})/k_{\mathrm{B}}T]$, and N_{C}, E_{T}, and E_{C} are the effective density of states for the conduction band, the energy level of the trap, and the energy level of the conduction-band, respectively. The second part of the equation follows from the definition of k_{n} as a total recombination coefficient, $k_{\mathrm{n}} \equiv -\frac{dn}{dt}/n^2 = (1 + k_{\mathrm{rad}}\tau_{\mathrm{SRH,p}}n_1)/(\tau_{\mathrm{SRH,p}}n_1)$. The recombination coefficient k_{n} for the decay of electrons is importantly not the same as the recombination coefficient k_{p} for holes as the trapping will create an asymmetry between electron and hole densities. However, the two parameters will be closely related, that is, if we define k_{p} via $-dp/dt = k_{\mathrm{p}}p^2$, then $k_{\mathrm{p}} = (1 + k_{\mathrm{rad}}\tau_{\mathrm{SRH,p}}n_1)/(\tau_{\mathrm{SRH,p}}N_{\mathrm{t}}) = k_{\mathrm{n}}n_1/N_{\mathrm{t}}$, where N_{t} is the trap density (see Figure S13, Supporting Information for more information). The important feature of Equation (7) is that neither k_{n} nor k_{p} depends on the electron or hole density in the case of bimolecular recombination. The solution for the time-dependent electron density now becomes

$$n\,(t) = \frac{n\,(0)}{1 + n\,(0)\,k_{\mathrm{n}}t} \approx \frac{1}{k_{\mathrm{n}}t} \tag{8}$$

where the $\approx$ sign requires $n(0)k_{\mathrm{n}}t$ to be sufficiently large to be able to neglect the 1 in the denominator, which happens at long times, $t \gg (n(0)k_{\mathrm{n}})^{-1}$, or alternatively high fluences. A similar equation could be written down for the hole density. Thus, the dependence of carrier density on time is the same as for purely radiative recombination (see Equation (4)) but the meaning of the recombination coefficient has changed. While k_{rad} represented radiative recombination only, k_{n} represents both radiative band-to-band recombination and non-radiative recombination via shallow traps.

Thus, we have now established that the decay of $n(t)$ after a laser pulse could follow an exponential decay if deep traps dominate or a power-law decay if either radiative recombination or shallow defects dominate. **Figure 1** depicts the schematic of the charge carrier kinetics for all the cases. Furthermore, for low fluences and shorter times ($t \ll (n(0)k_{\mathrm{n}})^{-1}$), it could follow the unabbreviated version of Equation (8) that includes the "+1" in the denominator. These effects can be superimposed, whereby the power law should be relevant at higher carrier densities and the exponential decay visible at lower carrier densities. If we observe a power law at longer times after the pulse, we expect that $n(t) \propto 1/t$ and – for an intrinsic semiconductor – the photoluminescence intensity $\phi_{\mathrm{PL}}(t) \propto 1/t^2$. Other slopes would not follow from the simple model outlined above.

Given the shortcomings of studying power-law recombination with the methodology of exponential decays, it is a valid approach to attempt to determine experimental bimolecular recombination coefficients also directly from experimental data. To quantitatively evaluate the recombination, we define a bimolecular

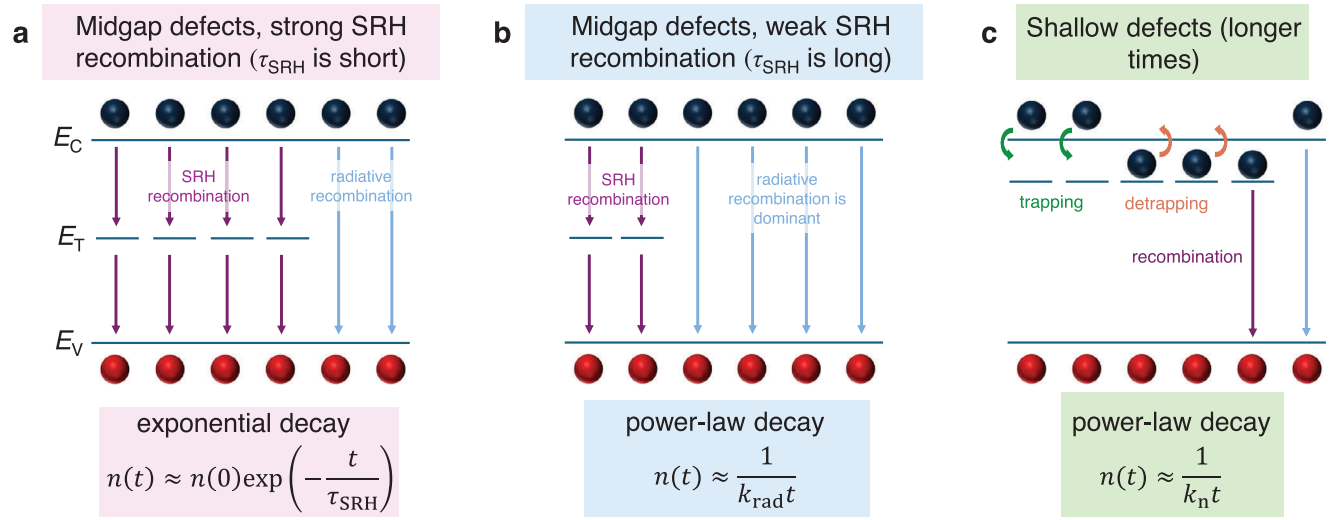

Figure 1. Schematic diagram of charge carrier kinetics of a) deep-trap dominated recombination, b) radiative recombination dominated and c) shallow-trap dominated recombination in a semiconductor film. Auger recombination is neglected for simplicity. In case of deep-trap dominated recombination, the carrier density decays exponentially if the non-radiative recombination is high. The decay only follows a power law relation when the non-radiative recombination is (extremely) low and the overall decay is dominated by radiative recombination. When shallow traps dominate, detrapping cannot be ignored, which complicates the charge carrier dynamics. This leads to the situation that at longer times (or alternatively higher fluences), the carrier density follows a power law decay.

recombination coefficient k_{diff}, which is calculated by the following equation,

$$k_{diff} = -\frac{1}{2\sqrt{np}} \cdot \frac{d\ln\phi_{PL}}{dt} \tag{9}$$

where n, p is the electron, hole concentration, respectively. For the definition of k_{diff} we only used quantities accessible by tr-PL such as the PL intensity and the np-product but did not use quantities such as n and p individually that are inaccessible. The meaning of k_{diff} and its relation to k_n and k_p are discussed in Note S2 (Supporting Information).

3. Results

3.1. Experimental Observation of Power-Law Decays in Lead-Halide Perovskite Films

Having established the possibility of power-law decays due to non-radiative recombination, we now study a variety of experimental data on perovskite films that are measured with a high dynamic range. **Figure** 2a shows the normalized decay curves of four different typical lead-halide perovskites. We observe that all the decays are consistent with a power-law decay rather than an exponential decay at long delay times, indicating that shallow traps dominate the recombination dynamics while truly exponential decays are absent even if the data is measured over six to nine orders of magnitude dynamic range. However, at the early stage of the decays (e.g., the first 50 ns depicted in Figure 2a), the decays can hardly follow a power-law relation. According to Equation (8), the $n(t)$ only exhibits power-law decay when $n(0)k_n t \gg 1$, which is challenging to satisfy at early times (i.e., t is small). Thus, not only the time and the recombination coefficient but also the initial carrier concentration affects $n(t)$ at early times.

We can now determine the differential decay times of these power-law decays using an approach described previously.[17] We use Equation (5) to calculate the decay times and plot them as a function of the Fermi-level splitting ΔE_F, which represents the injection level that is changing as a function of time during the measurement. This approach is suited to compare data taken with different fluences as shown in ref. [14,17] The initial Fermi level splitting just after the laser pulse ($t = 0$) is hereby estimated using $\Delta E_F(t = 0) = k_B T \ln(\Delta n(0) 2/n_i^2)$, where $\Delta n(0)$ is the initial carrier density estimated from the laser power density and n_i is the intrinsic carrier density. For later times, we know that $\Delta E_F(t) - \Delta E_F(0) = k_B T \ln(\phi_{PL}(t)/\phi_{PL}(0))$, that is, every order of magnitude drop in PL intensity leads to a reduction in Fermi-level splitting of $k_B T \ln(10)$. We use the Fermi level splitting as the x-axis instead of the carrier concentration because the ratio $\Delta n(t)/\Delta p(t)$ may be changing during the transient. In addition, the Fermi-level splitting ΔE_F with unit eV enables easier comparisons with voltages; that is, it is straightforward to determine the differential decay time at voltages that correspond to V_{oc} or V_{mpp} in a solar cell. Furthermore, it is straightforward to compare optical techniques such as tr-PL with electrical techniques as shown, for instance, in ref. [20]

In Figure 2b, all samples show a continuously increasing τ_{diff}, which is varying several orders of magnitude from high to low Fermi-level splitting ΔE_F. The different sets of τ_{diff} values are changing with an approximately constant slope, where $\tau_{diff} \propto \exp(-\Delta E_F/(2k_B T))$, as indicated by the dashed line. If any type of power law recombination dominates, we expect $\tau_{diff} = 1/(kn(t))$ to hold and hence $\tau_{diff} \propto \exp(-\Delta E_F/(2k_B T))$. While this could be an indication of radiative recombination, we conclude that it is likely affected by non-radiative recombination that is quadratic in electron density such as recombination via shallow defects.

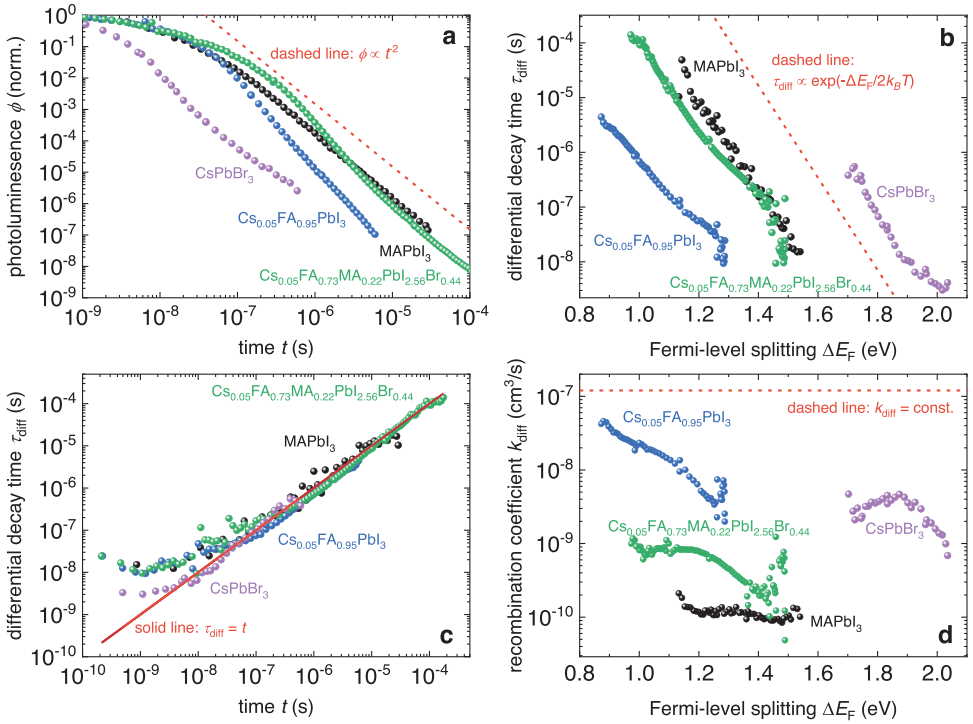

Figure 2. a) Normalized PL decays of perovskite films on a double-logarithmic scale measured using high fluences of 7.2 μJ cm^{-2} ($MAPbI_3$, MA is Methylammonium), 2.83 μJ cm^{-2} ($Cs_{0.05}FA_{0.73}MA_{0.22}PbI_{2.56}Br_{0.44}$, FA is Formamidinium), 2.74 μJ cm^{-2} ($CsPbBr_3$) and 0.78 μJ cm^{-2} ($Cs_{0.05}FA_{0.95}PbI_3$). Reference line $\phi \propto t^{-2}$ is plotted for comparison. b) Differential decay time τ_{diff} versus Fermi-level splitting ΔE_F corresponding to the decays shown in (a). Reference line $\tau \propto \exp(-\Delta E_F/(2k_B T))$ is shown for comparison. c) Decay times, τ_{diff} plotted as a function of time t. The solid line indicates the relation $\tau_{diff} = t$. d) Bimolecular recombination coefficient k_{diff} versus ΔE_F of different perovskite samples. The red lines indicate the behavior of bimolecular recombination at long times. The experimental data of $MAPbI_3$ film (the initial carrier concentration $n(0) \approx 7 \times 10^{17}$ cm^{-3}) were redrawn from ref. [17]. The structure is glass/$MAPbI_3$/n-trioctylphosphine oxide (TOPO).The experimental data of $Cs_{0.05}FA_{0.95}PbI_3$ ($n(0) \approx 3 \times 10^{16}$ cm^{-3}), $CsPbBr_3$ ($n(0) \approx 8 \times 10^{16}$ cm^{-3}) and $Cs_{0.05}FA_{0.73}MA_{0.22}PbI_{2.56}Br_{0.44}$ ($n(0) \approx 10^{17}$ cm^{-3}) were redrawn from ref. [14]. The structures are glass/$Cs_{0.05}FA_{0.95}PbI_3$, glass/$CsPbBr_3$, and glass/poly (methyl methacrylate)/$Cs_{0.05}FA_{0.73}MA_{0.22}PbI_{2.56}Br_{0.44}$/n-octylammonium iodide (OAI), respectively. All experimental data were measured by gated CCD (charge-coupled device) tr-PL setup.

In Figure 2c, the same decay times are now plotted versus the delay time leading to the rather unpleasant result that all points are placed around the line of $\tau_{diff} = t$. To understand this finding, let us consider the case of a power-law decay and combine Equation (4) with $\tau_{diff} = 1/(kn(t))$ for any arbitrary recombination coefficient k to

$$\tau_{diff} = \frac{1}{n(0)\,k} + t \approx t \tag{10}$$

where the ≈ sign holds at longer times. Here, the term "longer times" is mathematically defined as $t \gg (n(0)k)^{-1}$ which implies that it is a function of the recombination coefficient k, the initial carrier concentration $n(0)$ and in consequence the fluence. We must understand that in the situation, where the decay is described by a power law, all information on the material properties is contained in k (see Equation (7)); hence k is what we want to determine. Whereas τ_{diff} plotted versus carrier density n or Fermi level splitting still contains the information on k, once τ_{diff} is plotted versus time, n disappears, k cancels out at longer times, and no information is left as long as the conditions for the ≈ sign in Equation (10) are met. Thus, the four curves in Figure 2c still contain the qualitative information that they originate from a power-law decay but at long times no quantitative information on the material properties remains. A further consequence of the continuously changing decay time is that extracting a constant lifetime no longer makes sense. Note that the clear correlation of τ_{diff} with time as shown in Figure 2c is a consequence of using data obtained with rather high fluences such that the condition $t \gg (n(0)k)^{-1}$ is met over most of the time range shown. If data is obtained with lower fluences, the first term in Equation (10) would become more important and the lifetime would be a function of fluence rather than of delay time. Additional discussion is provided in Figures S4 and S5 (Supporting Information). In Figure 2d, the PL decays were used to calculate the bimolecular recombination coefficient k_{diff} using Equation (9) which is plotted versus Fermi-level splitting. We observe that the variation range of k_{diff} is mostly within 1 order of magnitude, which is much smaller than that of τ_{diff}. For $MAPbI_3$, the values of k_{diff} are quite constant over the full range and for $Cs_{0.05}FA_{0.73}MA_{0.22}PbI_{2.56}Br_{0.44}$ in the low Fermi-level splitting region (corresponding to long times), which makes it possible to extract a representative value for quantitative comparison. Both display a low value of k_{diff}, suggesting a low degree of recombination loss. This is consistent with the high photoluminescence quantum yields Q_e^{lum} results (for $MAPbI_3$, $Q_e^{lum} \approx 12\%$, and

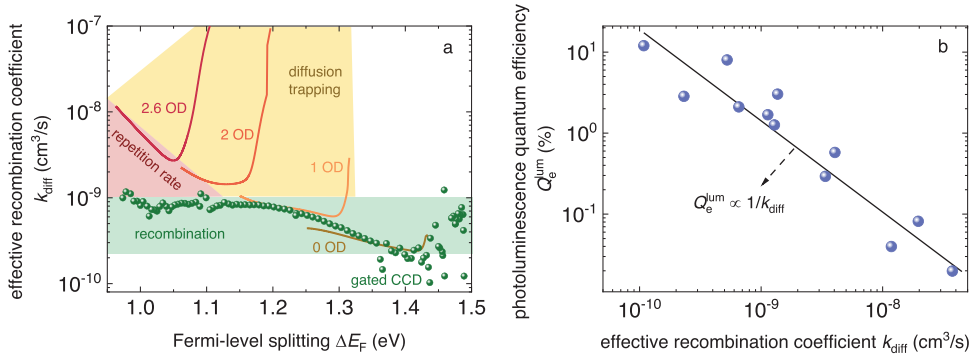

Figure 3. a) The bimolecular recombination coefficient k_{diff} versus Fermi-level splitting ΔE_F of perovskite film measuring from both TCSPC and gated CCD setups. The light red triangle indicates the region restricted by the repetition rate and tail subtraction method. The yellow area is affected by early time effects such as diffusion and trap filling. The green region is primarily affected by recombination. The data were redrawn from ref. [14] and $n(0)$ are $\approx 10^{17}$ cm^{-3} (gated CCD), 5×10^{16} cm^{-3} (0 OD), 5×10^{15} cm^{-3} (1 OD), 5×10^{14} cm^{-3} (2 OD), 1.3×10^{14} cm^{-3} (2.6 OD), respectively. The sample structure is glass/PMMA/$Cs_{0.05}FA_{0.73}MA_{0.22}PbI_{2.56}Br_{0.44}$/OAI. b) Meta-analysis of photoluminescence quantum efficiency Q_e^{lum} data from either Figure 2 or some of our earlier papers[5b,14,17] or our homemade perovskite film versus k_{diff} (see Table S5, Supporting Information). The data includes films, layer stacks as well as complete devices. The solid line indicates the relation of $Q_e^{lum} \propto 1/k_{diff}$. Please note that the same ΔE_F was used to acquire Q_e^{lum} and k_{diff} as they are both a function of ΔE_F.

for $Cs_{0.05}FA_{0.73}MA_{0.22}PbI_{2.56}Br_{0.44}$, $Q_e^{lum} \approx 2\%$), which will be discussed later. From Equation (S10) (Supporting Information), we know that k_{diff} is independent of the carrier concentration when shallow defects dominate the recombination, as indicated by the dashed line, and therefore, these cases are well described by shallow traps. We conclude that the relatively constant behavior of k_{diff} with carrier density or Fermi-level splitting indicates that the lead halide perovskites shown in Figure 2 do not possess deep defects, but rather shallow defects close to the band edges. The smaller k_{diff} signifies shallower energy levels and lower hole capture coefficient for the traps in case of the traps are close to the conduction band.[14] In contrast, if the traps are close to the valence band, then the electron capture coefficient should be lower.

3.2. Recombination Coefficients and Luminescence Quantum Efficiencies

In **Figure 3a**, we compare the calculated k_{diff} using the data measured from the TCSPC and gated CCD setups for one sample. To enlarge the dynamic range, the TCSPC measurements were performed under different laser intensities (we used different optical density (OD) filters to adjust the intensities) and then merged. We observe that the envelope parts of curves from the TCSPC setup matched well with the data from the gated CCD setup in the ΔE_F range of 1.15–1.43 eV (region highlighted in green). Nevertheless, there is an obvious discrepancy at low Fermi-level splitting (0.95–1.15 eV, highlighted in red), which is caused by the repetition rate limitation and will be discussed later. At higher Fermi-level splittings, there is a region highlighted in yellow, where the TCSPC data is still affected by diffusion and possibly trapping effects, and therefore leads to a different apparent recombination coefficient for every fluence. Figure 3b shows the meta-analysis of photoluminescence quantum yields Q_e^{lum} as function of k_{diff} of our samples (see Table S5, Supporting Information), which exhibits a clear inverse relationship and thus indicates that k_{diff} is a good figure of merit for charge-carrier recombination in lead-halide perovskites. The $MAPbI_3$ sample exhibited the highest $Q_e^{lum} = 12\%$ and the lowest $k_{diff} = 1.08 \times 10^{-10}$ cm^3 s^{-1}, indicating an excellent defect passivation, and thus consequently showing a high V_{oc} for the corresponding device.[5b,17] Additionally, the triple-cation $Cs_{0.05}FA_{0.73}MA_{0.22}PbI_{2.56}Br_{0.44}$ sample presenting a long-lived photoluminescence decay and a low $k_{diff} = 6.56 \times 10^{-10}$ cm^3 s^{-1} also possessed a high $Q_e^{lum} = 2.11\%$.[14] The relationship $Q_e^{lum} = R_{rad}/R_{tot} \propto {k_{diff}}^{-1}$ can be illustrated by recalling that the total recombination in steady-state is described by $R_{tot} = k_{eff}\, np \propto k_{diff} np$ (see Figure S13, Supporting Information), whereby the proportionality sign is valid once (during the course of a tr-PL measurement) the initial phase of trap filling is over and the rates of trapping and detrapping toward the nearest band have become similar. In Figure S11 (Supporting Information), we show that k_{diff} can be effectively used for sample-to-sample comparison as it exhibits a difference in magnitude for the sample with and without defect passivation.

3.3. Importance of Repetition Rates for Analyzing Power-Law Decays

A further consequence of the scaling $\tau_{diff} = t$ is that the maximum obtained decay time τ_{diff} scales with the time window over which the decay is observed. This time window depends either on the repetition rate of the laser or the time at which the measured counts become indistinguishable from the background noise. Therefore, it makes sense to study the impact of the repetition rate and the background subtraction method in more detail. Some effects of high repetition rates have already been highlighted in the literature.[11c,21] Two well-known consequences of a TCSPC measurement are the pile-up effect and the dead-time-related signal distortion.[22] The pile-up effect originates from the fact that a single TCSPC channel can only record one photon per signal period. It can be avoided by maintaining a much lower count rate than the repetition rate. The dead-time-related signal distortion happens if the repetition rate is faster than the dead time of the detector used. We assume that these measurement distortions are well-understood and are handled

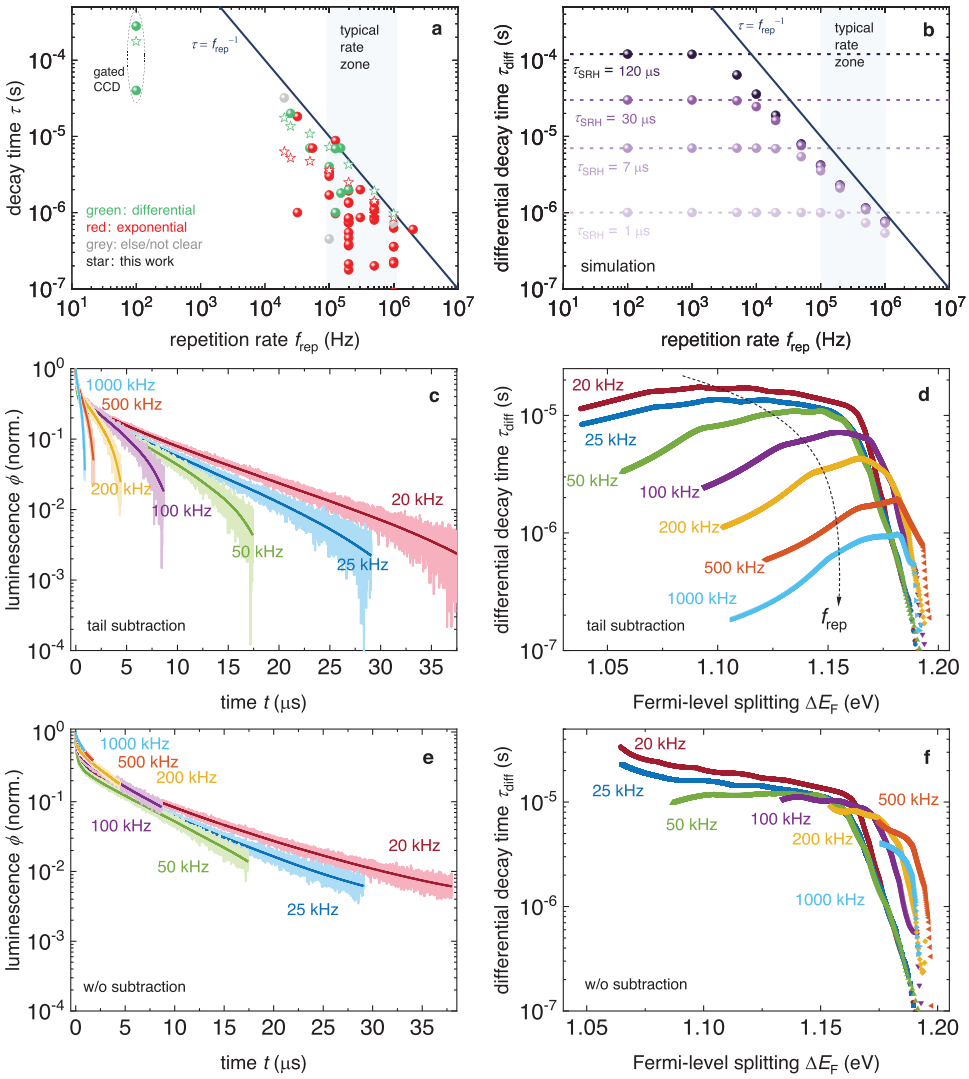

Figure 4. a) Meta-analysis of reported and in-house measured decay times as a function of the repetition rate. The solid red star data points correspond to our perovskite film using bi-exponential fitting, while the blue points correspond to the differential method with same sample. b) Simulated relationship between repetition rate and extracted differential PL decay time τ_{diff} as a function of SRH lifetime (of deep traps). The initial carrier concentration $n(0) = 10^{17}$ cm^{-3} was used. We subtracted non-existing noise from the simulated data using the tail subtraction method. Data without noise subtraction is shown in Figure S20 (Supporting Information). c) Normalized PL decay curves and d) extracted differential decay time τ_{diff} versus Fermi-level splitting of a homemade perovskite film utilizing the tail subtraction method. e) Normalized PL decay curves and f) differential decay time τ_{diff} versus Fermi-level splitting ΔE_F curves of perovskite film without any background subtraction. The structure is glass/PMMA/$Cs_{0.05}FA_{0.73}MA_{0.22}PbI_{2.56}Br_{0.44}$/OAI. The measurements were performed with different repetition rates using TCSPC setup where $n(0) \approx 5 \times 10^{14}$ cm^{-3} (the specific values are listed in Table 1).

with care. Another – more physical – effect may arise from a high density of residual charge carriers[23] in the perovskite when the next laser pulse arrives[11c,21]; therefore, effectively increasing the charge carrier density at time 0. Due to the non-linear charge carrier dynamics of the intrinsic perovskites this can lead to a change in the PL decay. Regardless, the community largely neglects the importance of the repetition rate to the degree that it is not even reported in an overwhelming number of cases. A meta-analysis of halide perovskite papers in the journals Science, Nature, Nature Energy, and Nature Photonics reveals that < 30% of the papers in 2021 and 2022 that report tr-PL data also report the repetition rate in the methods section (see Note S6, Supporting Information). **Figure** 4a shows the data of the literature included this information as well as our own measurements, where the decay times are determined using either a bi-exponential fit or the differential approach and plotted against the repetition rate f_{rep}. We can clearly observe an inverse relationship, where the determined decay times closely follow the inverse repetition rate. Exceptions include data points using a gated CCD setup with an extremely slow 100 Hz repetition rate. Both bi-exponential and differential methods show the same tendency; nevertheless, the exponentially fitted decay time τ_{bi} is generally lower than the differential decay time τ_{diff}, which is partly because the exponential fitting cannot properly fit decays with a large dynamic range (Note S1, Supporting Information). This finding can have several explanations. One possibility is that the samples had indeed

deep defects and therefore exponential decays and the repetition rate was adjusted to resolve the full decay in a time-efficient manner. Then the repetition rate would also scale inversely with the decay time. However, our findings in Figure 2 suggest that non-exponential decays are a feature of lead halide perovskites that can be observed over a wide range of compositions. Another possible reason is the above-mentioned relationship $\tau_{diff} = t$ that holds for bimolecular recombination after long times. Choosing a repetition rate f_{rep} will therefore limit the maximum decay time to $\tau_{diff} = 1/f_{rep}$. For this to be true, the delay time $1/f_{rep}$ needs to be longer than diffusion and trapping effects as well as longer than $1/(n(0)k)$. The dependence on $n(0)$ shows that the time after which $\tau_{diff} = t$ is valid, depends on the laser fluence and hence on a measurement parameter. Additionally, this condition depends on the recombination coefficient of the sample. As can be seen in Figure S5 (Supporting Information) for our sample, the condition can be fulfilled already after tens of ns for high fluences or only after tens of µs for low fluences. At lower times t, the decay time τ_{diff} can be higher than t. As TCSPC measurements are often carried out at low fluences[24] and high repetition rates,[25] we assume that the $\tau_{diff} = t$ relation is only responsible for a subset of the data shown in Figure 4a. Nevertheless, it is important to be aware of seemingly less important, technical aspects of measurements that can have a large influence on the interpretation of data and the generation of physical insights.

3.4. Background Subtraction and Apparent Exponential Decays

In tr-PL measurements, the signal may decay below the background level for earlier times than $1/f_{rep}$. This background level is often taken into consideration by including a constant y_0 in multi-exponential fits via $y = y_0 + \sum_i A_i e^{-x/\tau_i}$. Due to the continuously changing decay time, it may however be difficult in some cases to distinguish a long-lived decay from the background level. Thus, the constant y_0 can swallow part of the decay data and disturb the data analysis. We study the effect of such a background fitting by using the differential decay time method. The analog to background fitting is something we call tail subtraction. Here, the end of the decay curve just before the next pulse is averaged, and the mean is subtracted from the decay data. Figure 4b rationalizes the findings of Figure 4a by showing a theoretical relationship between the differential decay time τ_{diff} and repetition rate in the simple scenario of radiative recombination combined with a deep defect with a variable charge-carrier lifetime as given in the figure. By simulating the data until the inverse repetition rate and subtracting the apparent noise level (i.e., tail subtraction), we create many data points where the τ_{diff} is approximately determined by $1/(2f_{rep})$ rather than by the actual SRH lifetime. Once the extracted τ_{diff} is significantly shorter than $1/(2f_{rep})$, we would however expect to be able to determine the correct SRH lifetime (for deep trap) from the extracted τ_{diff}.

Figure 4c illustrates the implications of the tail subtraction for an OAI post-treated triple-cation perovskite film with a composition of $Cs_{0.05}FA_{0.73}MA_{0.22}PbI_{2.56}Br_{0.44}$. We measured tr-PL using repetition rates ranging from 20 kHz to 1 MHz using the TCSPC setup and 100 Hz using the gated CCD setup (see Figure S3, Supporting Information). The data were cut at a signal-to-noise ratio of 1 to avoid overinterpretation of the noisy part of the decay. Furthermore, the background was considered by subtracting the noise level observed before the pulse, that is, tail subtraction as discussed in Note S4 (Supporting Information). For faster repetition rates, the decay appears S-shaped, that is, bends down for longer times, while for slower repetition rates, we observe a mono-exponential decay over most of the time axis. However, such mono-exponential decay is an artifact caused by the cut-off operation. Without the cutoff operation, the raw curves measured by slower repetition rates also showed an S-shape, like that with faster repetition rates (see Figure S15, Supporting Information). Figure 4d shows the differential decay times as a function of Fermi-level splitting. We note that τ_{diff} might be interpreted as constant approaching ≈20 µs for slow f_{rep}, whereas they stay below 1 µs for faster repetition rates. At high ΔE_F, the τ_{diff} are generally shorter owing to the higher order components of the decay, such as radiative recombination, trap filling, or diffusion. At lower ΔE_F, the τ_{diff} become shorter again for fast f_{rep} because too much background is subtracted in these cases (see the discussion in Notes S4 and S5, Supporting Information). Note that for the 100 Hz data, the τ_{diff} increase to >100 µs (Figure S3, Supporting Information), where the measurable decay time is not limited by f_{rep} but by the dynamic range of the measurement setup. It follows that even a repetition rate of 20 kHz is too high. Thus, for a range of repetition rates from 1 MHz to 100 Hz, the extracted τ_{diff} varies by more than a factor of 100, whereby all the data measured using TCSPC result in $\tau \approx 1/(2f_{rep})$ (see the data points highlighted in red and blue in Figure 4a). The discrepancy observed at different frequencies is attributed to the improper use of the tail subtraction method. When we did not use any subtraction (denoted as "w/o sub." in the figures), the decay curves and the τ_{diff} versus ΔE_F plots with different repetition rates exhibited improved alignment (Figure 4e,f). Furthermore, we observed that the use of the tail subtraction method could lead to erroneous sample-to-sample comparisons, as demonstrated in Figures S17–S19 (Supporting Information).

To illustrate the effect of the subtraction method, we compare three typical noise subtraction methods, that is, tail subtraction, (real) background subtraction, and the case without subtraction using numerical simulations. As shown in **Figure 5**a, the black curve is the artificial noise spectrum, which cannot be neglected because it is comparable to the PL signal at longer times. In this case, the PL decay curve is the sum of the PL signal and the noise at long times when nothing has been subtracted, resulting in a slower decrease at long times (w/o sub., blue curve). Meanwhile, the τ_{diff} exhibits an increasing trend in the low ΔE_F region (Figure 5b). In contrast, the curve shows the opposite trend (that is, S-shaped decay) when using the tail subtraction method (purple curve). In this case, only the results obtained using background subtraction (green curves) were reliable. In Figure S21 (Supporting Information) (Note S5, Supporting Information), we experimentally demonstrate this phenomenon using our home-made perovskite sample. Therefore, a proper noise subtraction method is important for interpreting tr-PL data and should be employed depending on the measurement conditions. Although background subtraction is always the most reliable method, it is usually time-consuming. Fortunately, there are some hints for choosing the subtraction method that can be observed during the measurement, which are discussed in Note S5 (Supporting Information). In brief, tail subtraction can only be effective when

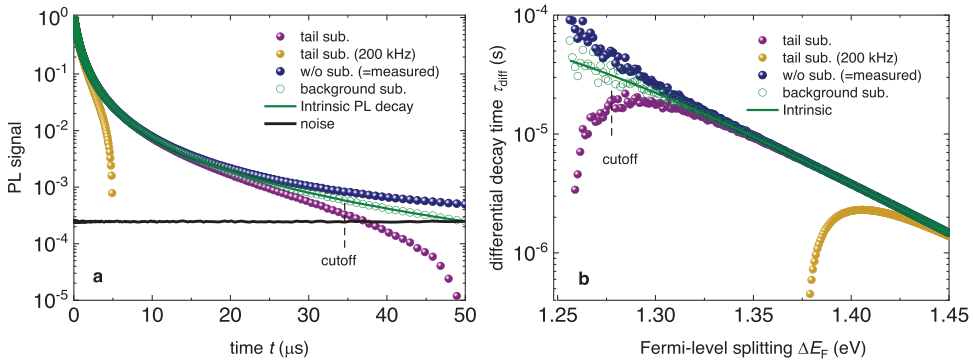

Figure 5. Comparison of the simulated results of a) PL decay curves and b) τ_{diff} versus ΔE_F curves using three different subtraction methods. The default repetition rate is 20 kHz, the initial carrier concentration is $n(0) = 10^{17}$ cm^{-3}, radiative recombination coefficient $k_{rad} = 10^{-11}$ cm^{3}s^{-1}, and $\tau_{SRH} = 120$ μs. The simulation and calculation details are given in the Methods Section.

the tail of decay really hits the noise (for samples with a short decay time), while "without subtraction" can only be valid when the real background noise is much lower than the PL signal of the tail (for sample with long decay time). In other cases, only background subtraction is valid, which means that additional noise measurements are needed under the same circumstances. The tail shape of the PL decay curve can help determine the relative relationship between the PL signal and noise (see Figures S22–S24, Supporting Information). The simulations also support the experimental results shown in Figure 4c,d. Tail subtraction leads to an S-shaped decay, which is more obvious at higher repetition rates. In the actual measurement, the lower the repetition rate, the lower the signal-to-noise ratio, and thus, the greater the effect of noise. This implies that a larger fraction of the tail part of the curve is cut off. If we assume that the 20 kHz curve will be cut off at 35 μs, then the remaining part may be mistaken as mono-exponential decay, and thus a plateau will appear in the low ΔE_F region in the τ_{diff} versus ΔE_F plot.

4. Discussion

Lead-halide perovskites are known for their extremely low doping density,[12] and the theoretical prediction of a high density of shallow defects but a low density of deep defects.[14] As recombination via shallow defects in an intrinsic semiconductor leads to power-law decays, the observation that these decays are present in a range of different perovskite compositions, as shown in Figure 2a, is a feature consistent with what we know about lead-halide perovskites. The challenge in detecting power-law decays is that they become visibly distinct from the popular multi-exponential decays only for data with a significant dynamic range. Thus, research on the consequences of power-law decays for the data analysis of PL transients is still in its early stages. This is understandable because the combination of a low doping density, shallow defects, and generally slow recombination is a rather unique feature in the world of optoelectronics. The most important consequence of power-law decays is that the concept of a decay time (or lifetime) that originates from the analysis of exponential decays becomes complex when applied to power laws. Here, we distinguish between two different situations. The determination of a differential decay time can still provide insights into the material properties if the data are plotted versus any assay of injection level, that is, either carrier density or Fermi-level splitting. However, when the data are plotted versus the delay time after the pulse, the decay time loses all information on the carrier density, and thereby the recombination coefficient is lost. This leads to two important issues with respect to the current approach of showing and analyzing tr-PL data. First, data without information on the carrier density may be meaningless. Second, decays fitted on a linear time axis using sums of exponential functions are likely to be strongly affected by the extent of the time axis, which is often set by the inverse repetition rate. Thus, while trends between samples may still survive, the absolute values of "lifetimes" obtained from tr-PL on lead-halide perovskites might be strongly affected by the chosen repetition rates. The fact that neither repetition rate nor fluence is typically specified prominently in the data or noted at all (particularly in the case of the repetition rate) makes it difficult to quantitatively compare published data.

One way out could be to move away from decay times as a figure of merit for those decays that indeed resemble a power law and that do not eventually approach an exponential decay. This requires several steps. First, a double-logarithmic plot of PL versus time will be helpful in identifying power laws. This can be combined with measurements at different fluences or measurements with a high dynamic range. In such situations, where a power law is observed, determination of the effective differential bimolecular recombination coefficient should allow the extraction of a figure of merit for recombination that does not vary by orders of magnitude as a function of fluence. Finally, background subtraction should be carefully considered to avoid both over- or underestimation of the noise and subsequently risk misinterpretation of the functional form of the PL decay.

5. Suggested Workflow

Based on the insights we have obtained so far, we want to briefly summarize how a workflow might look like that is considering the discussed issues with repetition rates, power-law decays, and background subtraction and that is focused on linking the experimental data to an interpretation based on physical models in a direct way. **Figure 6** provides a visualization of the workflow. The first step is the measurement of the data that can be done using either photon counting systems (TCSPC) or a gated CCD

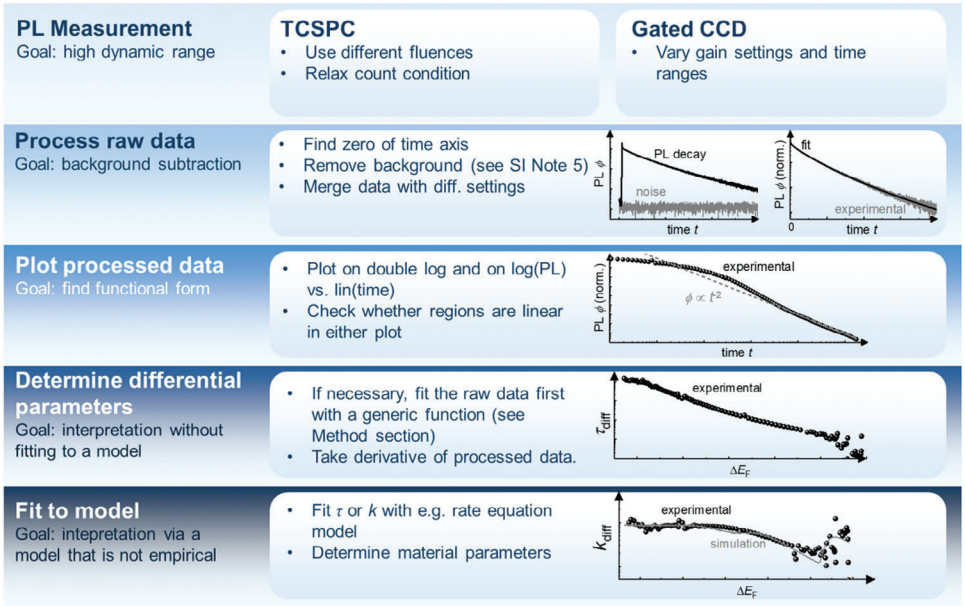

Figure 6. Workflow for the measuring, processing, plotting, and interpretation of transient photoluminescence data that is applicable to measurements via photon counting systems or gated CCD cameras. The goal is to identify the type of decay (rather exponential or power law), and then determine differential lifetimes or recombination coefficients (depending on the data) that can already be interpreted without invoking a model. In the last step, we suggest comparing the data to a model (e.g., by fitting) to infer parameters of the model such as capture coefficients or trap depths.

camera. No matter which approach is used for detection, the goal of this first step is to obtain data over a wide range of carrier densities and thereby to obtain a high dynamic range. This can always be achieved by varying the laser fluence over a wide range, which allows covering a range of carrier densities without requiring a huge dynamic range of any individual measurement. As the first tens to few hundreds of ns of a decay can be affected by diffusion effects,[26] it is however necessary for the measurement time for any given fluence to significantly exceed hundreds of ns. In case of the gated CCD camera or any system working with internal signal amplification, the gain of the amplification[17,20a] can be changed to obtain a higher dynamic range even without varying the fluence (see Figure 2).

The data processing step is necessary to find time zero of the decay (usually the time, where the counts have a maximum) and to subtract the background as explained in Section 3.4. In the case, measurements at different gain settings were taken, the data processing would also include merging these decays into one. After processing the raw data, we can now plot the data (PL vs time) to establish the character of the decay (e.g., power-law or exponential decay). Here, we recommend plotting the data both on a semilogarithmic and a double-logarithmic plot. If the data becomes a straight line on the double-logarithmic plot, it follows a power law. If this is not the case but the decay becomes linear on a semi-logarithmic curve, the data is rather following an exponential decay. Of course, mixtures of both situations are possible, where, for example, higher fluences follow a power law and lower fluences become more exponential. In situations like the ones in Figure 2, the plotting would already provide clear information on the type of the decay (power law) and would affect the strategy for the next steps.

For data interpretation, we have two options that can be used in combination. One can either determine differential decay times or recombination coefficients to interpret the data without invoking a specific model or one can fit the data with a numerical or analytical model. In the latter case, the choice of model may create a bias toward a certain result while in the former case, this wouldn't be the case. However, only the fitting would allow one to infer parameters of a model such as capture coefficients or trap depths. In Figure 6, the first approach is the model-free determination of differential parameters via numerically calculating the derivative of the raw data via Equations (5) and/or (9). The advantage of this approach is that it might directly yield effective decay times or recombination coefficients if parts of the decay are perfect exponentials or power laws. In these cases, effective parameters could be read out directly from the plot without having to assume a specific model (e.g., a rate equation model). This approach would be equivalent to the way lifetime data in silicon photovoltaics are usually presented.[27] The last step would be the actual fitting of the data with a model resulting in the quantification of the parameters of the model. Fitting requires assuming a certain model which could be a rate equation model (including trapping and detrapping) or even a transient drift-diffusion model. The material parameters inferred from the model could then for instance be reinserted in forward device models (e.g., in drift-diffusion simulators) and could be linked to device performance. Instead of traditional fitting also more advanced methods such as Bayesian inference could be used for parameter inference.[28]

6. Conclusion

Transient photoluminescence (tr-PL) is a commonly used method to study recombination in lead-halide perovskites.

However, the measurement and analysis of tr-PL data lacks a systematic workflow that supports and facilitates data interpretation. We observe that in many lead-halide perovskite films, PL decays measured at higher fluences follow a power-law relation between PL intensity and time, which we attribute to shallow defects. These power law decays result in continuously varying decay times as a function of time and injection level. While plotting the data versus injection level will still maintain information related to material properties, plotting the data versus time leads to a loss in information and can create an unwanted dependence of the extracted decay time on measurement conditions such as fluence and repetition rate. The overarching goal of the measurement is to learn about the materials without having measurement conditions affect the interpretation of the data. Thus, we propose a series of measures to avoid data misinterpretation and to create a facile workflow summarized in Figure 6 that results in a sound data interpretation independent of the type of setup or the properties of the sample.

7. Experimental Section

Materials and Film Preparation: The preparation processes generally follow the previous work reported in ref. [14]. Methylammonium iodide (MAI, Greatcell Solar), Formamidinium iodide (FAI, Greatcell Solar), Cesium iodide (CsI, Alfa Aesar, 99.9%), Lead(II) iodide (PbI_2, TCI, 99.99%), Lead bromide ($PbBr_2$, Sigma–Aldrich, 99.999%) *N*,*N*-dimethylformamide (DMF, Sigma–Aldrich, 99.8%) and dimethyl sulfoxide (DMSO, Sigma–Aldrich, ≥99.9%) were used to prepare the perovskite solution. To be specific, 0.06 M CsI, 0.264 M MAI, 0.876 M FAI, 0.264 M $PbBr_2$, and 0.936 M PbI_2 were mixed together in DMF: DMSO (3:1 volume ratio) solvent. $Cs_{0.05}FA_{0.73}MA_{0.22}PbI_{2.56}Br_{0.44}$ (1.2 M) perovskite precursor solution was prepared by stirring at 75 °C for ≈2 h. Tiny amounts of poly (methyl methacrylate) (PMMA, average M_w≈120 000 by GPC) were added to the precursor (≈0.06 mg mL^{-1}). Before use, the precursor was filtered with a 0.45 µm PTFE filter.

Two types of stacks are prepared for PL measurement. The first one consists of a structure comprising glass/PMMA/$Cs_{0.05}FA_{0.73}MA_{0.22}PbI_{2.56}Br_{0.44}$/OAI, and is referred to as Sample-LT, as it exhibits a very long differential decay time. The second one is composed of glass/ $Cs_{0.05}FA_{0.73}MA_{0.22}PbI_{2.56}Br_{0.44}$, and is referred to as Sample-ST, as it has a relatively shorter decay time. Corning bare glasses (2.0 × 2.0 cm^2) are used as substrates. They were ultrasonically cleaned with Seife HellmanexIII (2% in water, 50 °C), acetone (VWR Chemicals, 20 °C) and IPA (Sigma–Aldrich, 99.5%, 20 °C) for 20 min, respectively. Before being transferred into N_2-filled glovebox, the cleaned substrates were treated with oxygen plasma (Diener Zepto, 50 W, 13.56 MHz, 10 min). For the Sample-LT, a PMMA layer and an n-Octylammonium iodide (OAI, Greatcell Solar) layer were separately prepared on the lower and upper surfaces of the perovskite film to reduce the defect density at the interfaces. Specifically, a, PMMA/chlorobenzene (CB, Sigma–Aldrich, 99.8%) solution (20 mg mL^{-1}) was spin-coated onto bare glass at 3000 rpm for 25 s and then annealed at 100 °C for 10 min. The OAI was dissolved in isopropyl alcohol (IPA, Sigma–Aldrich, 99.5%) solution at a concentration of 2 mg mL^{-1}, and then ~100 µL solution was dynamically spin-coated on the perovskite film at 5000 rpm for 30 s, subsequently followed by annealing at 100 °C for 5 min. For Sample-ST, the perovskite film was directly prepared on the Corning glass without PMMA layer and was not coated with an OAI layer.

To prepare perovskite film, the precursor solution was dropped onto the substrate to fully cover it. Subsequently, spin-coating process at 4000 rpm for 15 s and 6000 rpm for 40 s was employed for Sample-LT, whereas that at 2000 rpm for 30 s and 6000 rpm for 40 s was used for Sample-ST. 20–25 s before the end of the spin process, ≈300 µL anisole (Sigma–Aldrich, 99.7%) was dripped onto the film. After the spin-coating process was completed, the films were annealed at 100 °C for 20 min. The entire preparation process was conducted in the glovebox.

Table 1. Laser energy density, calculated initial carrier concentration n_0, and initial Fermi-level splitting ΔE_F for different repetition rates. The film thickness was ≈500 nm. These parameters were used to calculate differential decay time τ_{diff}.

Repetition rate [kHz]	Laser energy density [nJcm^{-2}]	$n(t=0)$ [cm^{-3}]	Initial ΔE_F [eV]
20	7.945	5.040×10^{14}	1.1963
25	7.945	5.040×10^{14}	1.1963
50	8.098	5.137×10^{14}	1.1973
100	8.149	5.169×10^{14}	1.1976
200	8.251	5.233×10^{14}	1.1983
500	8.352	5.298×10^{14}	1.1989
1000	7.334	4.652×10^{14}	1.1922

In addition to Sample-LT and Sample-ST, samples were also prepared with transport layers and electrodes. For the hole-transport layer, 1 mmol L^{-1} Me-PACz (TCI, > 99.0%)/Ethyl alcohol (VWR Chemicals, max 0.003% water) solution was spin-coated on ITO glass (Kinetic 2.0 × 2.0 cm^2) with 3000 rpm for 25 s. The as-prepared films were then heated at 100 °C for 10 min. Additionally, 25 nm C_{60} (Lumtec) and 8 nm bathocuproine (TCI, > 99.0%) layers were prepared by thermal evaporation at a rate of 0.1 Å s^{-1}. 80 nm silver were also prepared by thermal evaporation and the rate is 2 Å s^{-1}.

Transient Photoluminescence Measurement: A TCSPC setup equipped with a 640 nm laser (EPL-640 from Edinburgh Instrument Ltd.) and a detector (H10330C-45-C3 from Hamamatsu) was used for transient photoluminescence measurements with a temporal resolution of 2 ns. The laser spot size was 50 µm in diameter. The repetition rates were adjusted from 1000 to 20 kHz. The detailed information of laser energy density, n_0 and initial ΔE_F for each repetition rate is listed in **Table 1**. With the decrease in the repetition rate, the measurement times were adjusted from 250 s to a maximum of 9000 s. For the background noise measurement, the sample was taken out while other conditions remained the same as the corresponding PL measurement, including the lightproof sample holder. All measurements were performed in a black box to avoid stray light issues.

For the gated CCD setup, a 343 nm laser (FLARE NX 343) was used. The repetition rate, spot diameter, and light intensity were 100 Hz, 3.07 mm, and 4.73 µJ cm^{-2}, respectively. The calculated carrier concentration and ΔE_F at $t = 0$ are 1.8×10^{17} cm^{-3} and 1.49 eV, respectively. An intensified CCD camera (iStar DH720 from Andor Solis) with a spectrometer (SPEX 270 M from Horiba Jobin Yvon) was used to detect the emitted PL signal.

Steady-State Photoluminescence Measurement: The photoluminescence quantum efficiency Q_e^{lum} of the homemade perovskite film sample was acquired from steady-state photoluminescence measurement using a setup from QYB Quantum Yield Berlin GmbH (LP20-32). The measurement was conducted with a 532 nm laser under 1 sun illumination. The spot size is 0.1 cm^2. During the measurements, dark spectra were taken before each illuminated measurement to subtract the background.

Decay Time Extractions: Exponential fit and differential approach are used to extract the decay time from transient photoluminescence decay curves in the work. The raw data were cut at a signal-to-noise ratio of 1 to avoid overinterpretation of the noisy part of the decay. For exponential methods, equation $y = \sum_i A_i e^{-x/\tau_i}$ (i = 1, 2, 3, corresponding mono-, bi- and tri- exponential fitting) is used to fit the curve. Then, $\tau = \sum_i A_i \tau_i^2 / \sum_i A_i \tau_i$ is used to acquire a value as decay time.[8a] For the differential approach, the objective is to plot the τ_{diff} versusΔE_F and k_{diff} versusΔE_F figures which are deduced from the Φ_{PL} versus t data.[17] To do that, τ_{diff} is calculated from $\tau_{diff} = \left(-\frac{1}{2}\frac{d\ln(\phi_{PL})}{dt}\right)^{-1}$ and k_{diff} from $k_{diff} = -\frac{1}{2\sqrt{np}} \cdot \frac{d\ln(\phi_{PL})}{dt}$. The data obtained from the TCSPC setup has many points that lay close to each other with strong relative noise which

is amplified by the derivative of this data. A generic fit describing the data (but no physics) is generated by least squares spline fitting the $\log(\phi_{PL})$ via the MATLAB function slmengine.[29] The constraints are a fixed initial point and a monotonically decaying curve. The knots are distributed so that more knots are at short times where the curve is more dynamic. Alternatively, rational functions of 4th and 5th degree can be used which however carry the danger of linearizing the end of the decay, leading to fictitious plateaus in the differential decay time. For the data from the gated CCD setup, the derivative is taken directly without post-processing. As for the ΔE_F, the initial point ($t = 0$) was first calculated using $\Delta E_F(0) = k_B T \ \ln(\Delta n(0) 2/n_i^2)$. This equation is only valid at $t = 0$. When $t > 0$, it may not hold as Δn may not equal to Δp anymore due to reasons such as photodoping or trapping. Note that shallow traps will be more likely to exist either close to the valance band or the conduction band but not symmetrical. The relation $\phi_{PL} \propto \exp(\Delta E_F/k_B T)$ was used to calculate the Fermi level splitting at times after 0.[30] After getting the τ_{diff} versusΔE_F plot, the plateau value of τ_{diff} at low ΔE_F region would be acquired as decay time because this valve will just equal to τ_{SRH} when deep traps dominate the decay.[17] Since no plateaus appear, the highest value of τ_{diff} is used.

Simulations: A custom-developed MATLAB code was used to perform the simulations. The initial carrier concentration was set at $n(0) = 1 \times 10^{17}$ cm^{-3} and the radiative recombination coefficient was established at $k_{rad} = 1 \times 10^{-11}$ cm^{3}s^{-1}. The repetition rates were varied from 20 to 1000 kHz. The simulation was based on Equation (2). The transient PL ϕ_{PL} can be described as $\phi_{PL} \propto n^2(t)$. A random noise spectrum was designated as a function of time and denoted it as $\phi_{PL}^{noise}(t)$. Consequently, the measured result should be $\phi_{PL}^{measured}(t) = \phi_{PL}(t) + \phi_{PL}^{noise}(t)$. Tail subtraction was employed as the default method unless otherwise specified. To simulate tail subtraction, the acquired transient PL $\phi_{PL}^{tail\ sub.}(t)$ can be written as $\phi_{PL}^{tail\ sub.}(t) = \phi_{PL}^{measured}(t) - \phi_{PL}^{measured}(\text{end}) = \phi_{PL}(t) - \phi_{PL}(\text{end})$. In addition, both (real) background subtraction and w/o subtraction were simulated, where $\phi_{PL}^{background\ sub.}(t) = \phi_{PL}^{measured}(t) - \phi_{PL}^{noise2}(t)$ and $\phi_{PL}^{w/o\ sub.}(t) = \phi_{PL}^{measured}(t) = \phi_{PL}(t) + \phi_{PL}^{noise}(t)$. The random noise $\phi_{PL}^{noise2}(t)$ which has the same average value as $\phi_{PL}^{noise}(t)$, was used to simulate a real experimental situation in which another noise measurement can never obtain the same noise spectra as that during PL measurement.

Supporting Information

Supporting Information is available from the Wiley Online Library or from the author.

Acknowledgements

The authors acknowledge funding by the Helmholtz Association via the POF IV funding, via the project "Beschleunigter Transfer der nächsten Generation von Solarzellen in die Massenfertigung – Zukunftstechnologie Tandem-Solarzellen", via the Helmholtz.AI project AISPA – AI-driven instantaneous solar cell property analysis as well as by the Deutsche Forschungsgemeinschaft (German Research Foundation) via the project "Correlating Defect Densities with Recombination Losses in Halide-Perovskite Solar Cells".

Open access funding enabled and organized by Projekt DEAL.

Conflict of Interest

The authors declare no competing interests.

Data Availability Statement

The data that used in the main text are available in https://zenodo.org/records/11084712. Further information and data are available from the authors upon request.

Keywords

bimolecular recombination, effective recombination coefficients, lead-halide perovskites, power-law decays, transient photoluminescence

Received: July 25, 2024
Revised: August 31, 2024
Published online: September 11, 2024

[1] a) M. A. Green, A. Ho-Baillie, H. J. Snaith, *Nat. Photonics.* **2014**, *8*, 506; b) Y. Rong, Y. Hu, A. Mei, H. Tan, M. I. Saidaminov, S. I. Seok, M. D. McGehee, E. H. Sargent, H. Han, *Science.* **2018**, *361*, eaat8235.

[2] a) D. Luo, R. Su, W. Zhang, Q. Gong, R. Zhu, *Nat. Rev. Mater.* **2020**, *5*, 44; b) S. D. Stranks, G. E. Eperon, G. Grancini, C. Menelaou, M. J. P. Alcocer, T. Leijtens, L. M. Herz, A. Petrozza, H. J. Snaith, *Science.* **2013**, *342*, 341; c) Q. Dong, Y. Fang, Y. Shao, P. Mulligan, J. Qiu, L. Cao, J. Huang, *Science.* **2015**, *347*, 967.

[3] a) A. Kojima, K. Teshima, Y. Shirai, T. Miyasaka, *J. Am. Chem. Soc.* **2009**, *131*, 6050; b) H.-S. Kim, C.-R. Lee, J.-H. Im, K.-B. Lee, T. Moehl, A. Marchioro, S.-J. Moon, R. Humphry-Baker, J.-H. Yum, J. E. Moser, M. Grätzel, N.-G. Park, *Sci. Rep.* **2012**, *2*, 591; c) S. Sidhik, Y. F. Wang, M. De Siena, R. Asadpour, A. J. Torma, T. Terlier, K. Ho, W. B. Li, A. B. Puthirath, X. T. Shuai, A. Agrawal, B. Traore, M. Jones, R. Giridharagopal, P. M. Ajayan, J. Strzalka, D. S. Ginger, C. Katan, M. A. Alam, J. Even, M. G. Kanatzidis, A. D. Mohite, *Science.* **2022**, *377*, 1425; d) A. K. Jena, A. Kulkarni, T. Miyasaka, *Chem. Rev.* **2019**, *119*, 3036.

[4] a) K. Wu, G. Liang, Q. Shang, Y. Ren, D. Kong, T. Lian, *J. Am. Chem. Soc.* **2015**, *137*, 12792; b) K. Lin, J. Xing, L. N. Quan, F. P. G. de Arquer, X. Gong, J. Lu, L. Xie, W. Zhao, D. Zhang, C. Yan, W. Li, X. Liu, Y. Lu, J. Kirman, E. H. Sargent, Q. Xiong, Z. Wei, *Nature.* **2018**, *562*, 245; c) I. L. Braly, D. W. deQuilettes, L. M. Pazos-Outón, S. Burke, M. E. Ziffer, D. S. Ginger, H. W. Hillhouse, *Nat. Photonics.* **2018**, *12*, 355.

[5] a) L. Krückemeier, U. Rau, M. Stolterfoht, T. Kirchartz, *Adv. Energy Mater.* **2020**, *10*, 1902573; b) Z. F. Liu, L. Krückemeier, B. Krogmeier, B. Klingebiel, J. A. Márquez, S. Levcenko, S. Öz, S. Mathur, U. Rau, T. Unold, T. Kirchartz, *ACS Energy Lett.* **2019**, *4*, 110; c) Z. Liu, J. Siekmann, B. Klingebiel, U. Rau, T. Kirchartz, *Adv. Energy Mater.* **2021**, *11*, 2003386.

[6] a) T. Kirchartz, J. A. Márquez, M. Stolterfoht, T. Unold, *Adv. Energy Mater.* **2020**, *10*, 1904134; b) C. M. Wolff, P. Caprioglio, M. Stolterfoht, D. Neher, *Adv. Mater.* **2019**, *31*, 1902762; c) M. Stolterfoht, V. M. Le Corre, M. Feuerstein, P. Caprioglio, L. J. A. Koster, D. Neher, *ACS Energy Lett.* **2019**, *4*, 2887; d) S. Feldmann, S. Macpherson, S. P. Senanayak, M. Abdi-Jalebi, J. P. H. Rivett, G. Nan, G. D. Tainter, T. A. S. Doherty, K. Frohna, E. Ringe, R. H. Friend, H. Sirringhaus, M. Saliba, D. Beljonne, S. D. Stranks, F. Deschler, *Nat. Photonics.* **2020**, *14*, 123; e) A. R. Bowman, S. Macpherson, A. Abfalterer, K. Frohna, S. Nagane, S. D. Stranks, *Phys. Rev. Appl.* **2022**, *17*, 044026; f) E. M. Hutter, T. Kirchartz, B. Ehrler, D. Cahen, E. Von Hauff, *Appl. Phys. Lett.* **2020**, *116*, 100501.

[7] a) R. A. Sinton, A. Cuevas, *Appl. Phys. Lett.* **1996**, *69*, 2510; b) S. Rein, T. Rehrl, W. Warta, S. W. Glunz, *J. Appl. Phys.* **2002**, *91*, 2059; c) S. Rein, *Lifetime Spectroscopy: A Method of Defect Characterization in Silicon for Photovoltaic Applications*, *85*, Springer Science & Business Media, Berlin/Heidelberg, Germany **2005**.

[8] a) J. Tong, Q. Jiang, A. J. Ferguson, A. F. Palmstrom, X. Wang, J. Hao, S. P. Dunfield, A. E. Louks, S. P. Harvey, C. Li, H. Lu, R. M. France, S. A. Johnson, F. Zhang, M. Yang, J. F. Geisz, M. D. McGehee, M. C. Beard, Y. Yan, D. Kuciauskas, J. J. Berry, K. Zhu, *Nat. Energy.* **2022**, *7*, 642; b) W. Li, M. U. Rothmann, Y. Zhu, W. Chen, C. Yang, Y. Yuan, Y. Y. Choo, X. Wen, Y.-B. Cheng, U. Bach, J. Etheridge, *Nat. Energy.* **2021**,

6, 624; c) S. Tan, T. Huang, I. Yavuz, R. Wang, T. W. Yoon, M. Xu, Q. Xing, K. Park, D.-K. Lee, C.-H. Chen, R. Zheng, T. Yoon, Y. Zhao, H.-C. Wang, D. Meng, J. Xue, Y. J. Song, X. Pan, N.-G. Park, J.-W. Lee, Y. Yang, *Nature*. **2022**, *605*, 268; d) H. Min, D. Y. Lee, J. Kim, G. Kim, K. S. Lee, J. Kim, M. J. Paik, Y. K. Kim, K. S. Kim, M. G. Kim, T. J. Shin, S. Il Seok, *Nature*. **2021**, *598*, 444; e) T. Huang, S. Tan, S. Nuryyeva, I. Yavuz, F. Babbe, Y. Zhao, M. Abdelsamie, M. H. Weber, R. Wang, K. N. Houk, C. M. Sutter-Fella, Y. Yang, *Sci. Adv.* **2021**, *7*, 1799; f) A. J. Barker, A. Sadhanala, F. Deschler, M. Gandini, S. P. Senanayak, P. M. Pearce, E. Mosconi, A. J. Pearson, Y. Wu, A. R. Srimath Kandada, T. Leijtens, F. De Angelis, S. E. Dutton, A. Petrozza, R. H. Friend, *ACS Energy Lett.* **2017**, *2*, 1416.

[9] L. Krückemeier, Z. Liu, B. Krogmeier, U. Rau, T. Kirchartz, *Adv. Energy Mater.* **2021**, *11*, 2102290.

[10] a) *Edinburgh Instruments, TCSPC – What Is Time-Correlated Single Photon Counting?* https://www.edinst.com/blog/what-is-tcspc/(accessed: April 2024); b) M. Wahl, *Time-Correlated Single Photon Counting (Technical Note of PicoQuant GmbH)* https://www.picoquant.com/images/uploads/page/files/7253/technote_tcspc.pdf (accessed: April 2024).

[11] a) A. Kiligaridis, P. A. Frantsuzov, A. Yangui, S. Seth, J. Li, Q. An, Y. Vaynzof, I. G. Scheblykin, *Nat. Commun.* **2021**, *12*, 3329; b) M. J. Trimpl, A. D. Wright, K. Schutt, L. R. V. Buizza, Z. P. Wang, M. B. Johnston, H. J. Snaith, P. Müller-Buschbaum, L. M. Herz, *Adv. Funct. Mater.* **2020**, *30*, 2004312; c) L. G. Kudriashova, D. Kiermasch, P. Rieder, M. Campbell, K. Tvingstedt, A. Baumann, G. V. Astakhov, V. Dyakonov, *J. Phys. Chem. Lett.* **2017**, *8*, 4698; d) E. V. Péan, M. L. Davies, *J. Chem. Inf. Model.* **2023**, *63*, 4477.

[12] F. Peña-Camargo, J. Thiesbrummel, H. Hempel, A. Musiienko, V. M. Le Corre, J. Diekmann, J. Warby, T. Unold, F. Lang, D. Neher, M. Stolterfoht, *Appl. Phys. Rev.* **2022**, *9*, 021409.

[13] C. L. Davies, M. R. Filip, J. B. Patel, T. W. Crothers, C. Verdi, A. D. Wright, R. L. Milot, F. Giustino, M. B. Johnston, L. M. Herz, *Nat. Commun.* **2018**, *9*, 293.

[14] Y. Yuan, G. Yan, C. Dreessen, T. Rudolph, M. Hulsbeck, B. Klingebiel, J. Ye, U. Rau, T. Kirchartz, *Nat. Mater.* **2024**, *23*, 391.

[15] F. Staub, I. Anusca, D. C. Lupascu, U. Rau, T. Kirchartz, *J. Phys.: Mater.* **2020**, *3*, 025003.

[16] a) J. Siekmann, A. Kulkarni, S. Akel, B. Klingebiel, M. Saliba, U. Rau, T. Kirchartz, *Adv. Energy Mater.* **2023**, *13*, 2300448; b) Y. M. Wang, S. Akel, B. Klingebiel, T. Kirchartz, *Adv. Energy Mater.* **2024**, *14*, 2302614.

[17] L. Krückemeier, B. Krogmeier, Z. Liu, U. Rau, T. Kirchartz, *Adv. Energy Mater.* **2021**, *11*, 2003489.

[18] W. Shockley, W. T. Read, *Phys. Rev.* **1952**, *87*, 835.

[19] A. Richter, S. W. Glunz, F. Werner, J. Schmidt, A. Cuevas, *Phys. Rev. B.* **2012**, *86*, 165202.

[20] S. Ravishankar, L. Kruppa, S. Jenatsch, G. H. Yan, Y. M. Wang, *Energ Environ Sci.* **2024**, *17*, 1229.

[21] M. J. Trimpl, A. D. Wright, K. Schutt, L. R. V. Buizza, Z. Wang, M. B. Johnston, H. J. Snaith, P. Müller-Buschbaum, L. M. Herz, *Adv. Funct. Mater.* **2020**, *30*, 2004312.

[22] a) W. Becker, in *Advanced Time-Correlated Single Photon Counting Techniques*, (Eds.: A. W. Castleman, J. P. Toennies, W. Zinth), Springer, Berlin, Heidelberg **2005**, Ch. 7.9; b) M. Patting, M. Wahl, P. Kapusta, R. Erdmann, *Dead-time effects in TCSPC data analysis, Photon Counting Applications, Quantum Optics, and Quantum Cryptography*, *6583*, SPIE, Bellingham, Washington USA, https://doi.org/10.1117/12.722804 (accessed: May 2007); c) L. Turgeman, D. Fixler, *J Biophotonics*. **2014**, *7*, 442; d) Picoquant GmbH, Pile-Up Effect, https://www.tcspc.com/doku.php/glossary:pile-up_effect (accessed: April 2024)

[23] a) A. Marunchenko, J. Kumar, A. Kiligaridis, D. Tatarinov, A. Pushkarev, Y. Vaynzof, I. G. Scheblykin, *ACS Energy Lett.* **2024**, *5*, 2075; b) A. Marunchenko, J. Kumar, A. Kiligaridis, S. M. Rao, D. Tatarinov, I. Matchenya, E. Sapozhnikova, R. Ji, O. Telschow, J. Brunner, A. Yulin, A. Pushkarev, Y. Vaynzof, I. G. Scheblykin, *J. Phys. Chem. Lett.* **2024**, *15*, 6256.

[24] a) E. Gutierrez-Partida, H. Hempel, S. Caicedo-Dávila, M. Raoufi, F. Peña-Camargo, M. Grischek, R. Gunder, J. Diekmann, P. Caprioglio, K. O. Brinkmann, H. Köbler, S. Albrecht, T. Riedl, A. Abate, D. Abou-Ras, T. Unold, D. Neher, M. Stolterfoht, *ACS Energy Lett.* **2021**, *6*, 1045; b) X. M. Zhao, T. R. Liu, Q. C. Burlingame, T. J. Liu, R. Holley, G. M. Cheng, N. Yao, F. Gao, Y. L. Loo, *Science*. **2022**, *377*, 307.

[25] a) S. G. Motti, J. B. Patel, R. D. J. Oliver, H. J. Snaith, M. B. Johnston, L. M. Herz, *Nat. Commun.* **2021**, *12*, 6955; b) P. Caprioglio, J. A. Smith, R. D. J. Oliver, A. Dasgupta, S. Choudhary, M. D. Farrar, A. J. Ramadan, Y.-H. Lin, M. G. Christoforo, J. M. Ball, J. Diekmann, J. Thiesbrummel, K.-A. Zaininger, X. Shen, M. B. Johnston, D. Neher, M. Stolterfoht, H. J. Snaith, *Nat. Commun.* **2023**, *14*, 932; c) A. J. Knight, A. D. Wright, J. B. Patel, D. P. McMeekin, H. J. Snaith, M. B. Johnston, L. M. Herz, *ACS Energy Lett.* **2019**, *4*, 75.

[26] C. Cho, S. Feldmann, K. M. Yeom, Y.-W. Jang, S. Kahmann, J.-Y. Huang, T. C. J. Yang, M. N. T. Khayyat, Y.-R. Wu, M. Choi, J. H. Noh, S. D. Stranks, N. C. Greenham, *Nat. Mater.* **2022**, *21*, 1388.

[27] a) R. Barrio, J. J. Gandía, J. Cárabe, N. González, I. Torres, D. Muñoz, C. Voz, *Sol. Energy Mater. Sol. Cells.* **2010**, *94*, 282; b) P. N. K. Deenapanray, M. Hörteis, D. Macdonald, K. J. Weber, *Electrochem Solid St.* **2005**, *8*, G78; c) J. Deckers, M. Debucquoy, R. Mertens, J. Poortmans, *Energy Procedia*. **2015**, *77*, 36; d) C. Fai, C. J. Hages, A. J. C. Ladd, *PRX Energy*. **2023**, *2*, 033013.

[28] a) C. Fai, G. A. Manoukian, J. B. Baxter, A. J. C. Ladd, C. J. Hages, presented at *2023 Ieee 50th Photovoltaic Specialists Conference, Pvsc*, , San Juan, PR, USA June **2023**; b) T. Kirchartz, B. Das, *J Phys-Energy*. **2023**, *5*, 031001; c) R. E. Brandt, R. C. Kurchin, V. Steinmann, D. Kitchaev, C. Roat, S. Levcenco, G. Ceder, T. Unold, T. Buonassisi, *Joule*. **2017**, *1*, 843; d) C. Fai, A. J. C. Ladd, C. J. Hages, *Joule*. **2022**, *6*, 2585.

[29] J. D'Errico, *MATLAB Central File Exchange, SLM – Shape Language Modeling*, https://www.mathworks.com/matlabcentral/fileexchange/24443-slm-shape-language-modeling (accessed: April 18 2024).

[30] P. Wurfel, *J. Phys. C Solid State*. **1982**, *15*, 3967.